UAV Integrity Monitoring Measure Improvement using Terrestrial Signals of Opportunity

Mahdi Maaref and Zaher M. Kassas
University of California, Irvine

BIOGRAPHIES

Mahdi Maaref received a B.S. and M.S. from the University of Tehran in 2008 and 2011, respectvely, and a Ph.D. in Electrical Engineering from Shahid Beheshti University, in 2016. He was a visiting research collaborator at the University of Alberta, Edmonton, Canada in 2016. Currently, he is a postdoctoral research fellow at the University of California, Irvine and a member of the Autonomous Systems Perception Intelligent and Navigation (ASPIN) Laboratory. His research interests include autonomous ground vehicles, opportunistic perception, and autonomous integrity monitoring.

Zaher (Zak) M. Kassas is an assistant professor at the University of California, Irvine and director of the ASPIN Laboratory. He received a B.E. in Electrical Engineering from the Lebanese American University, an M.S. in Electrical and Computer Engineering from The Ohio State University, and an M.S.E. in Aerospace Engineering and a Ph.D. in Electrical and Computer Engineering from The University of Texas at Austin. In 2018, he received the National Science Foundation (NSF) Faculty Early Career Development Program (CAREER) award, and in 2019, he received the Office of Naval Research (ONR) Young Investigator Program (YIP) award. His research interests include cyber-physical systems, estimation theory, navigation systems, autonomous vehicles, and intelligent transportation systems.

ABSTRACT

A method for improving the integrity monitoring measure of Global Positioning System (GPS) by exploiting terrestrial signals of opportunity (SOPs) is developed. The proposed method considers a receiver mounted on an unmanned aerial vehicle (UAV), which makes pseudorange observations on GPS satellites and terrestrial SOPs. First, SOP pseudorange measurement errors are characterized from an extensive data collected with a UAV in different environments: open sky, semi-urban, and urban. Next, the vertical protection level (VPL) reduction by exploiting terrestrial SOPs is studied. It is demonstrated that adding terrestrial SOP measurements, which are inherently at low elevation angles is more effective to reduce VPL over adding GPS measurements. Experimental results to evaluate the developed method are presented for a UAV navigating in an urban environment over a trajectory of 823 m, while collecting GPS signals and cellular real long-term evolution (LTE) SOPs. It is demonstrated that the proposed method reduces the VPL by 57.76% from the VPL of GPS-only.

I. INTRODUCTION

Unmanned aerial vehicles (UAVs) rely on a suite of sensors and actuators in order to control their motion, monitor their surrounding, and navigate safely. Global navigation satellite system (GNSS) is one of the main components of a UAV's navigation system. However, GNSS signals are jammable, spoofable, and may not be reliable in certain environments (e.g., indoors and deep urban canyons) [1, 2]. Integrity monitoring is one criterion to evaluate GNSS performance, and refers to the capability of the system to detect anomalies and warn the user when the system should not be used [3]. A high-integrity navigation system must be able to (i) detect and (ii) reject incorrect measurements and provide an integrity measure of the confidence in the system performance at any time [4].

The integrity of GNSS measurements can be obtained through the navigation message, which indicates the anomalies related to satellite operation such as the transmitters' clock errors and satellite service failure. However, the integrity information provided by the navigation message is not desirable for real-time applications as the ground control segment (GCS) requires a few hours to broadcast the failure [5]. Hence, integrity monitoring is usually obtained by means of additional frameworks. These frameworks are divided into internal and external categories [6]. External methods (e.g., ground based augmentation system (GBAS), satellite based augmentation system (SBAS), etc.)

leverage a network of ground monitoring stations to monitor the transmitted signals, while internal methods (e.g., receiver autonomous integrity monitoring (RAIM)) typically use the redundant information within the transmitted navigation signals. In contrast to external integrity monitoring methods, RAIM alleviates the need for costly, bulky, and computationally intensive infrastructures. RAIM detects pseudorange measurement faults by only exploiting the redundancy of GNSS signals to check the measurements' consistency [7].

Since the redundancy of measurements is essential for RAIM-based fault detection and exclusion, incorporating more measurements in a favorable transmitter-to-receiver geometry could significantly enhance the performance of integrity monitoring. Hence, the joint use of measurements provided by different GNSS satellite constellations, namely the multi-constellation approach, has been extensively studied in the literature [8–10]. In contrast to existing approaches in the literature, this paper considers exploiting terrestrial signals of opportunity (SOPs) as an additional "constellation" to improve integrity monitoring measures. SOPs are radio frequency (RF) signals that are not intended for navigation but can be exploited for navigation, especially in GNSS-challenged environments. SOPs are abundant in urban canyons and are free to use, making them desirable sources for navigation, either as a complement or an alternative to GNSS signals [11, 12]. Recent research have demonstrated how to exploit SOPs (e.g., cellular signals [13], digital television signals [14], AM/FM signals [15], and low Earth orbit satellite signals [16]) to produce a navigation solution in a standalone fashion and in an integrated fashion, aiding an inertial measurement unit (IMU) [17, 18] and lidar [19]. Moreover, the literature demonstrated the benefit of fusing SOP and GNSS signals to reduce the vertical dilution of precision (VDOP) [20, 21]. However, to the author's knowledge, this is the first paper that studies the enhancement in integrity monitoring measures by coupling SOP and Global Positioning System (GPS) signals.

This paper adopts the traditional GPS RAIM algorithm to incorporate terrestrial SOPs. The proposed algorithm provides improved performance with respect to the traditional RAIM algorithm by (i) increasing measurement redundancy and (ii) establishing favorable SOP-to-UAV geometry. This paper assesses the integrity monitoring performance by analyzing the UAV's vertical protection level (VPL). The protection level refers to a circular area centered at the user's real position, which assures to contain the estimated position with a probability equal or smaller than a pre-defined threshold, called the integrity risk [22].

Protection levels can be predicted using the transmitter-to-receiver geometry [4]. With the exception of GPS receivers mounted on high-flying UAVs, all GPS satellites are typically above the receiver. As a consequence, GPS satellite observables lack elevation angle diversity and the VPL of a GPS-only navigation solution is degraded. In the proposed framework, the elevation angle span may effectively double, as the UAV could fly above SOP transmitters. Hence, incorporating additional measurements obtained from terrestrial SOPs, not only enhances the RAIM performance by increasing redundant measurements, but also improves the protection levels by exploiting the inherently small elevation angles of terrestrial SOPs. Fig. 1 illustrates the proposed approach. As can be seen, the proposed approach differs from existing ground-based integrity monitoring approaches (e.g., GBAS), as it increases the measurement redundancy and improves the geometry without requiring installing dedicated, costly ground-based stations. Using the abundant and free-to-use terrestrial SOP transmitters, makes the proposed framework desirable for UAV navigation in the urban environments.

This paper considers the following problem. A UAV-mounted receiver navigating in an urban environment is assumed to make pseudorange observations on multiple GPS satellites and multiple terrestrial SOPs and to fuse these observations through an estimator. A modified RAIM approach is employed to calculate the VPL. This paper studies the enhancement in VPL by adding a varying number of SOPs, which are inherently at low elevation angles and provide a better transmitter-to-receiver geometry. This paper makes three contributions. First, a GPS-SOP RAIM framework for UAVs is developed. Second, the improvement in the integrity monitoring measures due to incorporating terrestrial SOP measurements is studied. Third, simulation and experimental results with cellular long-term evolution (LTE) SOPs are presented evaluating the efficacy of the proposed integrity monitoring framework on a UAV navigating in an urban environment. It is demonstrated that while the integrity monitoring measures are improved when additional observables from GPS satellites are used, adding SOP observables is more effective to tighten the VPL over adding GPS observables. The experimental results using GPS and 11 cellular SOPs show that the proposed framework reduces the VPL by 57.76%.

The structure of this paper is organized as follows. Section II formulates the GPS-SOP navigation solution. Section III studies empirically the salient attributes of cellular SOP measurements, namely accuracy, outliers, and failure
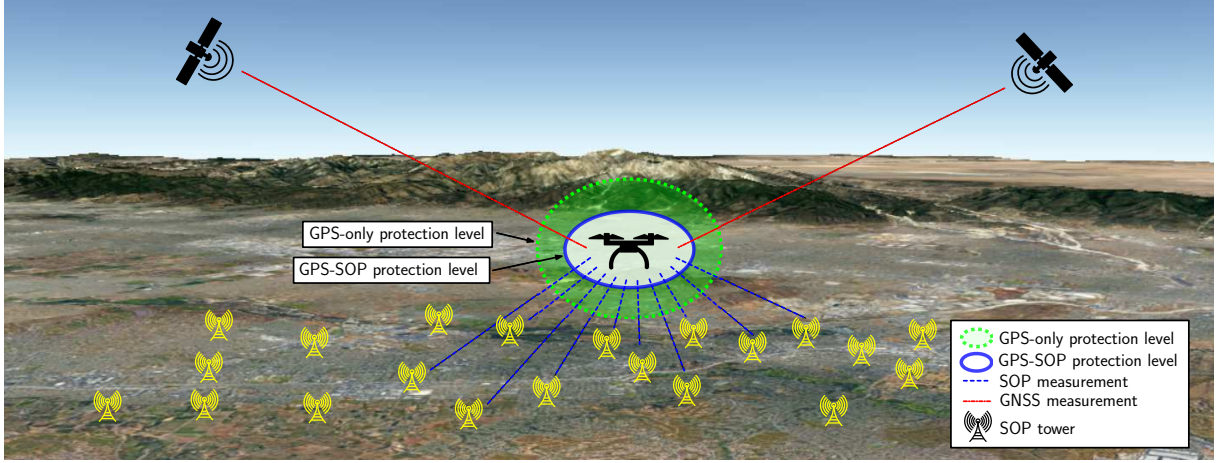
Fig. 1. The proposed method which combines pseudoranges obtained from GPS satellites and terrestrial SOP transmitters to enhance the integrity monitoring measures. Note the abundance of cellular LTE SOPs in this environment: Riverside, California, USA. Many other types of SOPs are also present in the environment but are not plotted here.

rate. This methodology can be applied to other terrestrial SOP classes. Section IV discusses the enhancement in the RAIM VPL by incorporating the SOP measurement. Section V presents simulation and experimental results with cellular LTE signals, evaluating the efficacy and accuracy of the proposed framework. Concluding remarks are given in Section VI.

II. NAVIGATION FRAMEWORK

This section formulates the UAV navigation framework. The environment is assumed to comprise N spatially-stationary SOP transmitters, denoted $\{S_n\}_{n=1}^{N}$. The location of SOP transmitters is assumed to be known *a priori*. This can be achieved via different approaches, such as satellite images, digital maps, cloud database, or radio mapping [23, 24]. The environment is also assumed to comprise M GPS satellites, denoted $\{G_m\}_{m=1}^{M}$. The UAV-mounted receiver makes pseudorange measurements to the M GPS satellites, denoted $\{z_{\mathrm{GPS_m}}\}_{m=1}^{M}$, and to the N SOP transmitters, denoted $\{z_{\mathrm{SOP_n}}\}_{n=1}^{N}$. These measurements are fused through a weighted nonlinear least-squares (WNLS) estimator to estimate the receiver's state vector $\boldsymbol{x}_r \triangleq \left[\boldsymbol{r}_r^{\mathsf{T}}, c\delta t_r\right]^{\mathsf{T}}$, where c is the speed of light, $\boldsymbol{r}_r \triangleq [x_r, y_r, z_r]^{\mathsf{T}}$ is the receiver's position, and δt_r is the receiver's clock bias.

The m-th GPS pseudorange measurement, after compensating for ionospheric and tropospheric delays, is modeled as

$$z'_{\mathrm{GPS_m}}(k) = \left\| \boldsymbol{r}_r(k) - \boldsymbol{r}_{\mathrm{GPS_m}}(k) \right\|_2 + c \cdot [\delta t_r(k) - \delta t_{\mathrm{GPS_m}}(k)] + v_{\mathrm{GPS_m}}(k),$$

where k is the time-step at which the pseudorange is drawn; $z'_{\mathrm{GPS_m}} \triangleq z_{\mathrm{GPS_m}} - c \cdot \delta t_{\mathrm{iono}} - c \cdot \delta t_{\mathrm{tropo}}$; $\boldsymbol{r}_{\mathrm{GPS_m}}$ and $\delta t_{\mathrm{GPS_m}}$ are the position and clock bias states of the m-th GPS satellite, respectively; δt_{iono} and $\delta t_{\mathrm{tropo}}$ are the ionospheric and tropospheric delays, respectively; and $v_{\mathrm{GPS_m}}$ is the GPS measurement noise, which is modeled as a zero-mean white Gaussian random sequence with variance $\sigma_{\mathrm{GPS_m}}^2$.

The n-th SOP pseudorange measurement, after mild approximations discussed in [25], is modeled as

$$z_{\mathrm{SOP_n}}(k) = \left\| \boldsymbol{r}_r(k) - \boldsymbol{r}_{\mathrm{SOP_n}}(k) \right\|_2 + c \cdot [\delta t_r(k) - \delta t_{\mathrm{SOP_n}}(k)] + v_{\mathrm{SOP_n}}(k),$$

where $\boldsymbol{r}_{\mathrm{SOP_n}}$ and $\delta t_{\mathrm{SOP_n}}$ are the position and clock bias states of the n-th SOP transmitter, respectively and $v_{\mathrm{SOP_n}}$ is the SOP measurement noise, which is modeled as a zero-mean white Gaussian random sequence with variance $\sigma_{\mathrm{SOP_n}}^2$. The clock biases $\{\delta t_{\mathrm{SOP_n}}\}_{n=1}^{N}$ are modeled as first-order polynomials, i.e., $\delta t_{\mathrm{SOP_n}}(k) = \dot{\delta t}_{\mathrm{SOP_n}} kT + \delta t_{\mathrm{SOP_{n,0}}}$, where $\dot{\delta t}_{\mathrm{SOP_n}}$ is the constant clock drift of the n-th transmitter and $\delta t_{\mathrm{SOP_{n,0}}}$ is the corresponding initial bias. More details about the first-order polynomial model of the SOP clock bias is discussed in [26–28].

The UAV-mounted receiver's state vector $\boldsymbol{x}_r$ is estimated from the measurement vector

$$\boldsymbol{z} \triangleq \left[z'_{\mathrm{GPS}_1}, \ldots, z'_{\mathrm{GPS}_M}, z_{\mathrm{SOP}_1}, \ldots, z_{\mathrm{SOP}_N} \right]^{\mathsf{T}},$$

through a WNLS estimator, given by

$$\boldsymbol{\Delta z} = \mathbf{H}\,\boldsymbol{\Delta x}_r + \boldsymbol{v},$$

where $\boldsymbol{\Delta z} \triangleq \boldsymbol{z} - \hat{\boldsymbol{z}}$ is the difference between the measurement vector $\boldsymbol{z}$ and its estimate $\hat{\boldsymbol{z}}$, $\boldsymbol{\Delta x}_r \triangleq \boldsymbol{x}_r - \hat{\boldsymbol{x}}_r$ is the difference between the receivers's state vector $\boldsymbol{x}_r$ and its estimate $\hat{\boldsymbol{x}}_r$, and $\boldsymbol{v} \triangleq \left[v_{\mathrm{GPS}_1}, \ldots, v_{\mathrm{GPS}_M}, v_{\mathrm{SOP}_1}, \ldots, v_{\mathrm{SOP}_N} \right]^{\mathsf{T}}$.

The measurement Jacobian used in the WNLS estimator is $\mathbf{H} \triangleq \left[\mathbf{H}_{\mathrm{GPS}}^{\mathsf{T}}, \mathbf{H}_{\mathrm{SOP}}^{\mathsf{T}} \right]^{\mathsf{T}}$, where

$$\mathbf{H}_{\mathrm{GPS}} \triangleq \begin{bmatrix} -\mathsf{c}(el_{\mathrm{GPS}_1})\mathsf{s}(az_{\mathrm{GPS}_1}) & -\mathsf{c}(el_{\mathrm{GPS}_1})\mathsf{c}(az_{\mathrm{GPS}_1}) & -\mathsf{s}(el_{\mathrm{GPS}_1}) & 1 \\ \vdots & \vdots & \vdots & \vdots \\ -\mathsf{c}(el_{\mathrm{GPS}_M})\mathsf{s}(az_{\mathrm{GPS}_M}) & -\mathsf{c}(el_{\mathrm{GPS}_M})\mathsf{c}(az_{\mathrm{GPS}_M}) & -\mathsf{s}(el_{\mathrm{GPS}_M}) & 1 \end{bmatrix},$$

$$\mathbf{H}_{\mathrm{SOP}} \triangleq \begin{bmatrix} -\mathsf{c}(el_{\mathrm{SOP}_1})\mathsf{s}(az_{\mathrm{SOP}_1}) & -\mathsf{c}(el_{\mathrm{SOP}_1})\mathsf{c}(az_{\mathrm{SOP}_1}) & -\mathsf{s}(el_{\mathrm{SOP}_1}) & 1 \\ \vdots & \vdots & \vdots & \vdots \\ -\mathsf{c}(el_{\mathrm{SOP}_N})\mathsf{s}(az_{\mathrm{SOP}_N}) & -\mathsf{c}(el_{\mathrm{SOP}_N})\mathsf{c}(az_{\mathrm{SOP}_N}) & -\mathsf{s}(el_{\mathrm{SOP}_N}) & 1 \end{bmatrix},$$

where $\mathsf{c}(\cdot)$ and $\mathsf{s}(\cdot)$ denote the cosine and sine functions, respectively; el_{GPS_m} and az_{GPS_m} are the elevation and azimuth angles of the m-th GPS satellites, respectively; and el_{SOP_n} and az_{SOP_n} are the elevation and azimuth angles of the n-th SOP transmitter, respectively. All elevation and azimuth angles are expressed in the East, North, Up (ENU) local coordinate frame, centered at the receiver's position. The weighting matrix in the WNLS is chosen as the inverse of the measurement noise covariance

$$\mathbf{R} = \mathrm{diag}\left[\sigma^2_{\mathrm{GPS}_1}, \ldots, \sigma^2_{\mathrm{GPS}_M}, \sigma^2_{\mathrm{SOP}_1}, \ldots, \sigma^2_{\mathrm{SOP}_N} \right],$$

where $\mathrm{diag}(\cdot)$ denote a diagonal matrix.

III. SOP PSEUDORANGE ERROR CHARACTERIZATION

In order to incorporate sop signals into RAIM frameworks (e.g., least squares (LS) RAIM, advanced RAIM (ARAIM), etc.), it is important to characterize the statistics of SOP signals as ranging measurements. Two important characteristics that must be evaluated are the accuracy and availability of SOP measurements. Accuracy refers to the degree of conformance of the measurements with the true ranges, while availability refers to the percentage of time that the measurements are usable by the navigator [4]. In contrast to GPS signals, SOP signals do not have publicly available records for their ranging performance. Therefore, the definition of fault for these measurements is still an open area of research. An initial study to analyze the statistics of cellular SOP pseudoranges for ground vehicle navigation was conducted in [28]. This paper extends [28] to characterize cellular SOP pseudoranges for UAV navigation. This methodology can be applied to other terrestrial SOP classes. In this paper, the data center of the Autonomous Systems Perception Intelligent and Navigation (ASPIN) Laboratory was used to statistically characterize the performance of cellular SOP pseudorange measurements. To collect this data, a UAV was flown for several hours, recoding cellular SOP pseudoranges. The pseudoranges were obtained using the Multichannel Adaptive TRansceiver Information eXtractor (MATRIX) software-defined reciever (SDR) discussed in [29–31] in several different (i) environments, including semi-urban and urban environments; (ii) carrier frequencies, and (iii) signal types, including LTE and code-division multiple access (CDMA) signals. Table I summarizes the characteristics of recorded cellular SOPs.

Next, the pseudorange measurements' errors were characterized using the method discussed in [28] via the following steps:

- **Step 1:** The true ranges between the receiver and SOP transmitter (i.e., $\left\| \boldsymbol{r}_r(k) - \boldsymbol{r}_{\mathrm{SOP}_n}(k) \right\|_2$) are removed from the recorded pseudoranges $z_{\mathrm{SOP}_n}(k)$. The true ranges are known *a priori* from the knowledge of the transmitters' location and receiver's ground truth position. The resulting measurement after removing the true range is given by:

$$z'_{\mathrm{SOP}_n}(k) \triangleq z_{\mathrm{SOP}_n}(k) - \left\| \boldsymbol{r}_r(k) - \boldsymbol{r}_{\mathrm{SOP}_n}(k) \right\|_2 = c \cdot \left[\delta t_r(k) - \delta t_{\mathrm{SOP}_n}(k) \right] + v_{\mathrm{SOP}_n}(k).$$

4

TABLE I

Environment	Number of Towers	Freq. [MHz]	Bandwidth [MHz]	Type	Date [DD/MM/YYYY]	Length [s]
Open sky and Semi-urban	2	882.75	1.23	CDMA	13/5/2017	345
	7	882.75	1.23	CDMA	22/2/2017	360
	8	882.75	1.23	CDMA	1/10/2017	200
	8	882.75	1.23	CDMA	1/10/2017	285
	2	882.75	1.23	CDMA	15/11/2017	365
Urban	11	739, 1955, 2125, 2145	10	LTE	16/6/2019	250

- **Step 2:** The error term due to the difference between the receiver's and the transmitter's clock biases (i.e., $c \cdot [\delta t_r(k) - \delta t_{\mathrm{SOP_n}}(k)]$) is removed from the measurement $z'_{\mathrm{SOP_n}}(k)$. To this end, a first-order polynomial approximation with a constant initial clock bias $c\delta t_{\mathrm{r,SOP_{n,0}}}$ and drift $c\dot{\delta} t_{\mathrm{r,SOP_{n,0}}}$ is used to model the difference between the receiver's and transmitter's clock biases, i.e.,

$$c \cdot [\delta t_r(k) - \delta t_{\mathrm{SOP_n}}(k)] = c\dot{\delta} t_{\mathrm{r,SOP_{n,0}}}\, kT + c\delta t_{\mathrm{r,SOP_{n,0}}},$$

where T is the sampling time. The constants $c\dot{\delta} t_{\mathrm{r,SOP_{n,0}}}$ and $c\delta t_{\mathrm{r,SOP_{n,0}}}$ are estimated by post-processing the recorded data from time-step 0 to time-step K via a least-squares (LS) estimator, which minimizes the cost function $\mathbf{G}$ given by

$$\mathbf{G} \triangleq \left(\left\| \boldsymbol{y} - \mathbf{S} \begin{bmatrix} c\dot{\delta} t_{\mathrm{r,SOP_{n,0}}} \\ c\delta t_{\mathrm{r,SOP_{n,0}}} \end{bmatrix} \right\|_2 \right)^2, \quad \mathbf{S} \triangleq \begin{bmatrix} 0 & T & \dots & KT \\ 1 & 1 & \dots & 1 \end{bmatrix}^{\mathsf{T}},$$

where the LS observation vector $\boldsymbol{y}$ is given by

$$\boldsymbol{y} \triangleq \left[z'_{\mathrm{SOP_n}}(0), \dots, z'_{\mathrm{SOP_n}}(K) \right]^{\mathsf{T}}.$$

The resulting measurement after removing the error due to clock bias difference is given by:

$$z''_{\mathrm{SOP_n}}(k) \triangleq z'_{\mathrm{SOP_n}}(k) - c\dot{\delta} t_{\mathrm{r,SOP_{n,0}}}\, kT - c\delta t_{\mathrm{r,SOP_{n,0}}} \simeq v_{\mathrm{SOP_n}}(k).$$

- **Step 3:** The sample mean and sample variance of the measurement error's probability density function (pdf) are calculated from

$$\hat{\mu}_{\mathrm{SOP_n}} = \frac{1}{K+1} \sum_{k=0}^{K} z''_{\mathrm{SOP_n}}(k), \quad \hat{\sigma}^2_{\mathrm{SOP_n}} = \frac{1}{K} \sum_{k=0}^{K} \left(z''_{\mathrm{SOP_n}}(k) - \hat{\mu}_{\mathrm{SOP_n}} \right)^2,$$

where $\mathbb{E}\{.\}$ is the expected value.

Fig. 2 illustrates the different environments in which the measurements were collected and the empirical pdfs found from the collected measurements. Overlayed on these pdfs are Gaussian pdfs with the calculated sample mean and sample variance. Table II summarizes $\hat{\mu}$ and $\hat{\sigma}$ in different environments.

Calculating the SOP measurements' availability is a more challenging problem as no official SOP measurement integrity standard has been issued yet. According to the Air Force GPS Standard Positioning Service Performance Standard (SPS PS) [32], the GPS measurement fault is defined by an error greater than 4.42 times the broadcast User Range Accuracy (URA). However, this cannot directly apply to SOP measurements since the SOP navigation message does not include URA information. Similar to the method discussed in [33], the SOP URA can be approximated using the collected empirical measurements. As shown earlier in this section, the SOP measurement error is generally

TABLE II

SAMPLE MEAN $\hat{\mu}$ AND SAMPLE VARIANCE $\hat{\sigma}$ OF GAUSSIAN PDFS OF PSEUDORANGE MEASUREMENT ERROR IN DIFFERENT ENVIRONMENTS

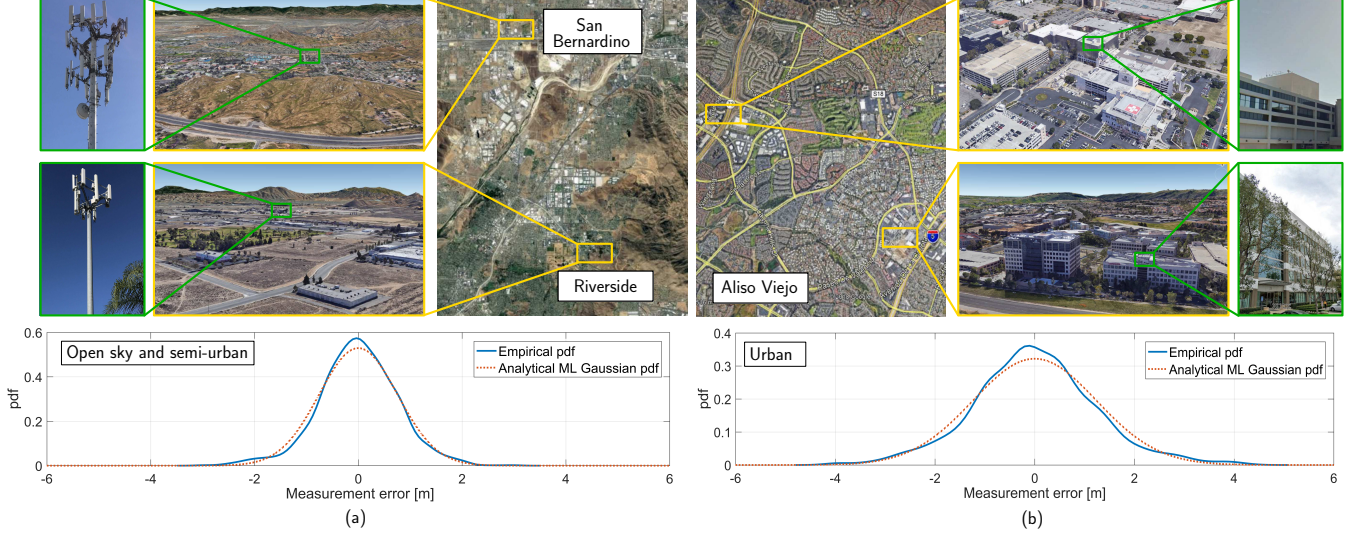| Environment	$\hat{\mu}$	$\hat{\sigma}$
Open sky and semi-urban	-3.66×10^{-18} m	0.75 m
Urban	7.10×10^{-18} m	1.23 m

Fig. 2. Characterization of cellular SOP pseudorange measurement accuracy in different environments in which the pseudoranges were collected. Empirical pdf of pseudorange errors and analytical Gaussian pdfs are illustrated for each environment: (a) Open sky and semi-urban and (b) urban.

less than 3 m. Therefore, it is possible to use 3 m as the SOP URA. Accordingly, an induced bias larger than 13.5 m can be considered as a fault and the probability of a cellular SOP transmitter being in a faulty state can be tentatively assumed to be 10^{-5}.

IV. VPL REDUCTION VIA ADDING SOPs

RAIM algorithms provide the user with an estimate of the confidence in the vertical position information via VPL. Several methods to calculate VPL have been proposed in the literature. Since all of these methods employ the transmitter-to-receiver geometry to construct the VPL, this paper considers a simple LS RAIM-based VPL [34] to study the effect of adding SOPs into the transmitter-to-receiver geometry. Formulating other types of RAIM for SOP-GPS framework is similar and could be investigated in future work.

The LS RAIM considers only one fault at each time, where a bias with magnitude b_i is added into the i-th pseudorange measurement. A hypothesis test, which considers residual test statistic can be formulated to detect a fault in the system according to

$$\varphi = \boldsymbol{r}^{\mathsf{T}} \mathbf{R}^{-1} \boldsymbol{r},$$

where $\boldsymbol{r}$ is the vector of pseudorange residuals ($\boldsymbol{r} = \boldsymbol{z} - \hat{\boldsymbol{z}}$). The resulting test statistic follows a central chi-squared distribution under fault-free operation and a non-central chi-squared distribution under faulty operation [35]. In both operations, the degrees of freedom is $d = N + M - 4$. The non-centrality parameter λ in faulty operation is given by

$$\lambda = \boldsymbol{b}^{\mathsf{T}} \mathbf{R}^{-1} (\mathbf{I} - \mathbf{B}) \boldsymbol{b},$$

where $\mathbf{I}$ is the identity matrix, $\boldsymbol{b} \triangleq [0, \ldots, 0, b_i, 0, \ldots, 0]^{\mathsf{T}}$ indicates the faulty measurement, and $\mathbf{B}$ is given by

$$\mathbf{B} \triangleq \mathbf{H}\big(\mathbf{H}^{\mathsf{T}} \mathbf{R}^{-1} \mathbf{H}\big)^{-1} \mathbf{H}^{\mathsf{T}} \mathbf{R}^{-1}.$$

The faulty operation's alarm is triggered if and only if the test statistic φ exceeds a threshold T_h, where the value of T_h may be obtained according to

$$P_{\text{FA}} = \int_{T_h}^{\infty} f_{\chi_d^2}(\tau)d\tau, \tag{1}$$

where P_{FA} is the probability of false alarm and $f_{\chi_d^2}$ is the chi-squared pdf with d degrees of freedom. Similarly, the non-centrality of the chi-squared distribution under a faulty operation that results in a probability of missed detection P_{MD} can be computed according to

$$P_{\text{MD}} = \int_0^{T_h} f_{\chi_d^2, \lambda_{\min}}(\tau)d\tau, \tag{2}$$

where $f_{\chi_d^2, \lambda_{\min}}$ represents the non-central chi-squared pdf with d degrees of freedom and non-centrality parameter $\lambda_{\min}$. It is important to note that P_{FA} and P_{MD} are pre-defined design parameters. Using (1) and (2), the value of T_h and $\lambda_{\min}$ can be obtained from a chi-square cumulative density function (cdf) table. Next, a parameter called slope_i is introduced to project the bias in the faulty measurement onto the vertical position error domain. The term slope_i depends on the transmitter-to-receiver geometry and is given by

$$\text{slope}_i = \frac{\|\mathbf{B}_{3i}\|\sqrt{\mathbf{R}_{ii}}}{\sqrt{\mathbf{S}_{ii}}},$$

where $\mathbf{S} \triangleq \mathbf{I} - \mathbf{B}$ and $\mathbf{X}_{ij}$ denotes the element of i-th row and j-th column of a matrix $\mathbf{X}$. The VPL is calculated as the projection onto the vertical position domain of the measurement bias that generates a non-centrality parameter equal to $\lambda_{\min}$ in the transmitter with the maximum slope [34], i.e.,

$$\text{VPL} = \text{slope}_{\max}\sqrt{\lambda_{\min}}, \quad \text{slope}_{\max} = \max_i \{\text{slope}_i\}, \quad i = 1, \dots, N + M.$$

It is important to note that when the slopes are large, a large vertical position error corresponds to a small error component in the test statistic. As a results, the RAIM is less likely able to detect the fault with probability equal to P_{MD}. Therefore, more favorable transmitter-to-user geometry is desirable to minimize $\text{slope}_{\max}$, to which the VPL is proportional.

Since all GPS satellites are typically above the UAV-mounted receiver, the GPS elevation angle range is theoretically limited between 0 and 90 degrees. Moreover, GPS receivers typically restrict the lowest elevation angle to some elevation mask, in order to ignore signals that are heavily degraded due to the ionosphere, troposphere, and multipath. In contrast to GPS-only approaches, the proposed SOP-GPS approach doubles the elevation angle range to -90 to 90 degrees, due to the fact that UAVs can fly directly above SOP transmitters. As a consequence, the proposed SOP-GPS approach increases the elevation angle diversity, which in turn improves the transmitter-to-receiver geometry and reduces the $\text{slope}_{\max}$ value.

To illustrate the VPL reduction by incorporating additional GPS measurements versus additional SOP measurements, a Monte Carlo simulation with 10^6 realizations was conducted. In each Monte Carlo realization, M GPS satellite azimuth and elevation angles were generated from uniform distributions over the interval $[-180, 180]$ degrees for the azimuth angles and the interval $[0, 90]$ degrees for the elevation angles. The GPS elevation angles were limited considering different elevation masks, i.e., 0, 5, 10, and 15 degrees. Then, an additional measurement at el_{new} and az_{new} was introduced. The azimuth angle of this additional measurement, az_{new}, was generated from uniform distribution over the interval $[-180, 180]$ degrees, while its elevation angle, el_{new}, was swept between -90 to 90 degrees. The reduction in the VPL due to adding an additional measurement was then recorded at each elevation angle. The corresponding VPL reduction for introducing an additional measurement at a sweeping elevation angle $-90 \leq el_{\text{new}} \leq 90$ degrees is plotted in Fig. 3 and Fig. 4 for different values of M and different GPS elevation mask.

The following may be concluded from these plots. First, while adding more measurements from other satellites decreases the VPL, it was observed that measurements from transmitters at low elevation angle are more effective in minimizing the VPL than transmitters at elevation angles between 0 and 90 degrees. Therefore, adding terrestrial SOP measurements, which are coming from transmitters at practically -90 to 0 degrees elevation angle range, minimize the VPL more than adding other GPS satellites. Second, in the environment with large GPS elevation
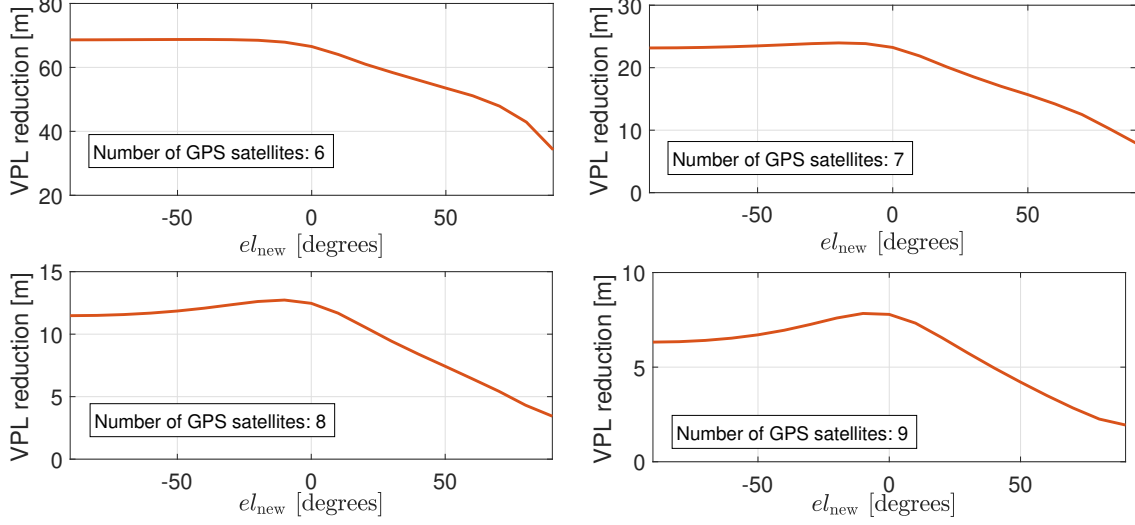
Fig. 3. The reduction in VPL after adding additional measurement at an elevation angle $-90 \leq el_{\text{new}} \leq 90$ degrees for $M = 6, \ldots, 9$.
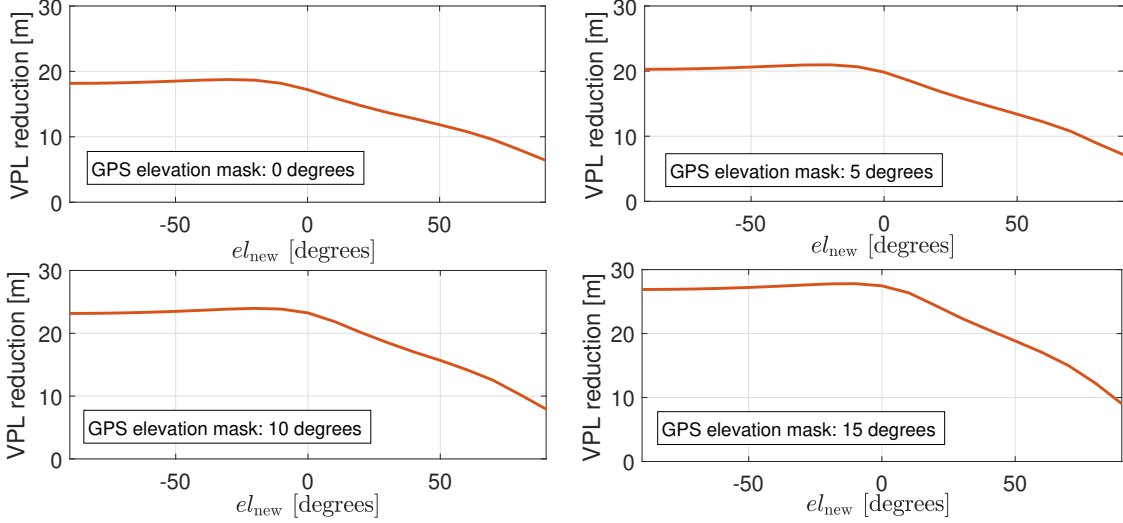

Fig. 4. The reduction in VPL after adding an additional measurement at an elevation angle $-90 \leq el_{\text{new}} \leq 90$ degrees for different elevation masks: 0, 5, 10, and 15 degrees. In this simulation, $M = 7$.

mask (e.g., deep urban canyon), the reduction in VPL due to adding SOP measurements is more significant than adding an additional GPS measurement. Third, in poor transmitter-to-receiver conditions where the receiver has LOS to only few GPS satellites, adding SOP measurements can significantly improve the transmitter-to-receiver geometry, compared to adding a new GPS measurements. Fourth, the VPL reduction values are comparable in the range of -90 to 0 degrees. This conveys an important conclusion that regardless of the UAV's flight height (whether above the SOPs or at the same height with respect to SOPs), this approach can provide the same VPL reduction.

V. EXPERIMENTAL RESULTS

A field test was conducted to demonstrate the efficacy of the proposed approach on a UAV. This section presents the hardware used in this experiment along with the experimental results.

8

A. Hardware Setup

A DJI Matrice 600 UAV was equipped with a dual-channel National Instrument (NI) universal software radio peripheral (USRP)-2955, driven by a GPSDO [36], to sample LTE SOPs. For this experiment, four LTE carrier frequencies were used: 739, 1955, 2125, and 2145 MHz. These frequencies are channels allocated for the USA cellular providers AT&T, T-Mobile, and Verizon. The sampling rate was set to 10 MSps, which was the LTE signals' bandwidth. The sampled LTE signals were saved on the computer and processed by MATRIX SDR [13, 30, 31], developed by the ASPIN Laboratory at the University of California, Irvine. The UAV was also equipped with a Septentrio AsteRx-i V integrated GNSS-IMU sensor [37]. Over the course of the experiment, the ground-truth trajectory of the UAV was obtained from this integrated GNSS-IMU navigation system, while the raw GPS measurements were used to estimate the receiver's position via the framework presented in Section II and to calculate the VPL via approach presented in Section IV. Septentrio's post-processing software development kit (PP-SDK) was used to process carrier phase observables collected by the AsteRx-i V and by a nearby differential GPS base station to obtain a carrier phase-based navigation solution. This integrated GNSS-IMU real-time kinematic (RTK) system was used to produce the ground-truth results with which the proposed navigation framework was compared. Fig. 5 illustrates the experimental hardware setup, the location of LTE transmitters, and the traversed trajectory.

Fig. 5. Experimental hardware setup and the traversed trajectory along with the position of cellular LTE SOP towers. A UAV was equipped with an integrated AsteRx-i V GNSS-IMU system, cellular antennas, and a USRP. The UAV traveled 823 m in an urban area (Irvine, California, USA) collecting GPS and cellular LTE signals from 11 cellular LTE SOP towers.

B. Experimental Results

The UAV flew for 240 s, while simultaneously listening to 11 LTE SOP transmitters. The GPS and cellular LTE pseudoranges were fed to a WNLS estimator, producing $\hat{x}_r$. Throughout the test, the fault detection test and VPL calculations were performed. The probability of false alarm for the outlier detection test was set to $P_{FA} = 0.005$ and the probability of missed detection was set to $P_{MD} = 0.0001$. Fig. 6 (a)–(b) show the sky plots of the transmitters available in the test environment for the GPS-only and GPS-SOP systems, respectively. Fig. 6 (c)–(d) shows the fault detection test, which compares the test statistic φ against the detection threshold T_h. Fig. 6 (e)–(f) shows the calculated VPL without and with incorporating the SOP signals, respectively, at a particular time instance (t = 100 s) during which the GPS-only VPL exceeds 23 m. The average GPS-only VPL over 240 s of flight was 22.21 m, whereas the average GPS-SOP VPL was 9.38 m. Hence, incorporating SOP transmitters reduces the VPL by 57.76%.
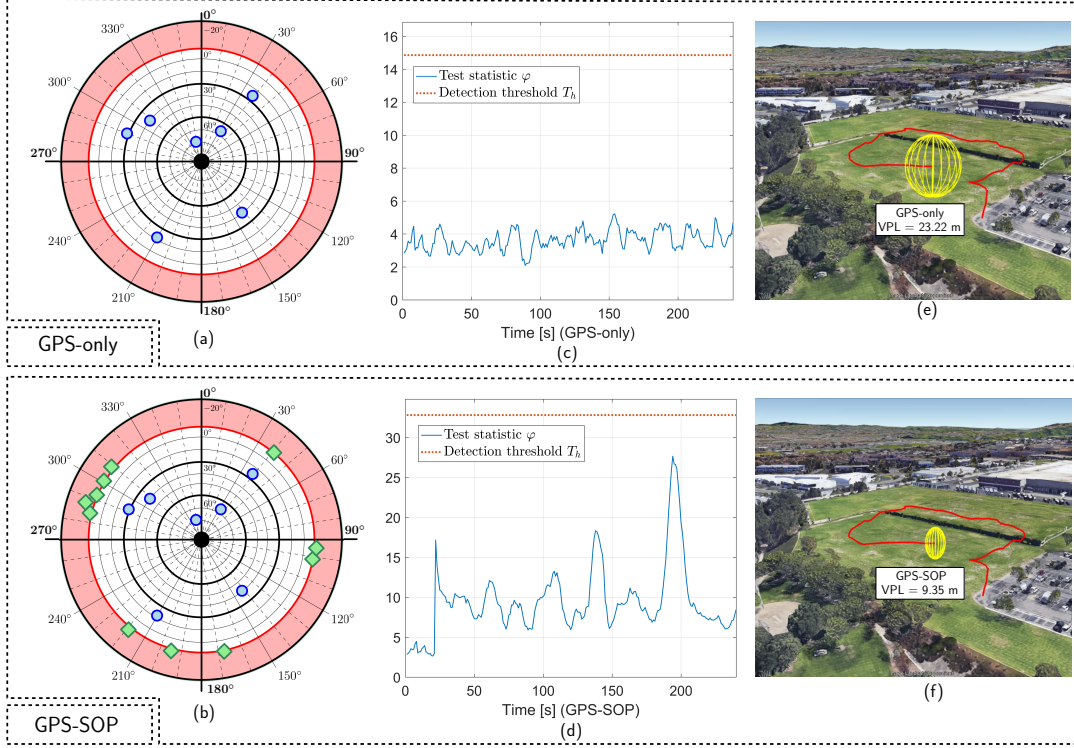
Fig. 6. Comparison between GPS-only and GPS-SOP frameworks: (a)–(b) Sky plots of the GPS and SOP transmitters available at the test environment, where the blue circles and the green circles represent GPS and SOP transmitters, respectively. (c)–(d) The test statistic φ and the detection threshold T_h for GPS-only and GPS-SOP frameworks. (e)–(f) A particular time instance during which the GPS-only VPL exceeds 23 m. It is evident from (f) that incorporating the SOP signals significantly reduces the VPL.

Table III compares VPL as well as the navigation performance of the proposed framework versus that of the GPS-only system.

TABLE III

COMPARISON BETWEEN NAVIGATION SOLUTION PERFORMANCE

Scenario	2-D RMSE [m]	3-D RMSE [m]	2-D Maximum error [m]	3-D Maximum error [m]	VPL [m]
GPS-only solution	2.34	4.37	9.11	18.08	22.21
GPS-sop solution	1.13	3.63	8.28	15.86	9.38
Improvement	51.46%	16.98%	9.14%	12.25%	57.76%

VI. CONCLUSION

This paper studied the reduction in a UAV's VPL of a GPS-based navigation solution by exploiting terrestrial SOPs. It was demonstrated that the VPL of the GPS-only solution can be reduced by exploiting the inherently small elevation angles of terrestrial SOPs. To this end, an LS RAIM was studied, which used the GPS measurements and the pseudorange measurements extracted from ambient SOP transmitters. Experimental results over a total traversed trajectory of 823 m validated the efficacy of the proposed framework and showed that the proposed framework significantly reduced the VPL, as it enables a full span of observation elevation angles. While this paper considered LS RAIM, more sophisticated RAIM algorithms, such as ARAIM, could be investigated in future work to account for multi-fault conditions.

ACKNOWLEDGEMENT

References

[1] J. Seo, Y. Chen, D. De Lorenzo, S. Lo, P. Enge, D. Akos, and J. Lee, "A real-time capable software-defined receiver using GPU for adaptive anti-jam GPS sensors," *Sensors*, vol. 11, no. 9, pp. 8966–8991, September 2011.

[2] B. Schnaufer, P. Hwang, J. Nadke, G. McGraw, and D. Venable, "Collaborative image navigation simulation and analysis for UAVs in GPS challenged conditions," in *Proceedings of IEEE/ION Position Location and Navigation Symposium*, April 2012, pp. 719–729.

[3] R. Toledo-Moreo, D. Betaille, and F. Peyret, "Lane-level integrity provision for navigation and map matching with GNSS, dead reckoning, and enhanced maps," *IEEE Transactions on Intelligent Transportation Systems*, vol. 11, no. 1, pp. 100–112, March 2010.

[4] N. Zhu, J. Marais, D. Betaille, and M. Berbineau, "GNSS position integrity in urban environments: A review of literature," *IEEE Transactions on Intelligent Transportation Systems*, pp. 1–17, January 2018.

[5] E. Kaplan and C. Hegarty, *Understanding* GPS*: Principles and Applications*, 2nd ed. Artech House, 2005.

[6] Q. Sun and J. Zhang, "RAIM method for improvement on GNSS reliability and integrity," in *Proceedings of Digital Avionics Systems*, October 2009, pp. 3–11.

[7] S. Bhattacharyya and D. Gebre-Egziabher, "Kalman filter-based RAIM for GNSS receivers," *IEEE Transactions on Aerospace and Electronic Systems*, vol. 51, no. 3, pp. 2444–2459, July 2015.

[8] M. Joerger, J. Neale, B. Pervan, and S. Datta-Barua, "Measurement error models and fault-detection algorithms for multi-constellation navigation systems," in *Proceedings of IEEE/ION Position, Location, and Navigation Symposium*, May 2010, pp. 927–946.

[9] D. Flament, D. Brocard, W. Ochieng, and C. Milner, "RAIM in dual frequency / multi constellation apv/lpv operations in aeronautics," in *Proceedings of Satellite Navigation Technologies and European Workshop on GNSS Signals and Signal Processing*, Dec 2010, pp. 1–7.

[10] G. Gopalakrishnan, F. Schmidt-Bruecken, and O. Kalden, "Simulation of integrity and availability of multi-constellation and multi-frequency GNSS augmentation systems," in *Proceedings of International Conference on Recent Advances in Space Technologies*, June 2013, pp. 1157–1162.

[11] J. Raquet and R. Martin, "Non-GNSS radio frequency navigation," in *Proceedings of IEEE International Conference on Acoustics, Speech and Signal Processing*, March 2008, pp. 5308–5311.

[12] Z. Kassas, "Collaborative opportunistic navigation," *IEEE Aerospace and Electronic Systems Magazine*, vol. 28, no. 6, pp. 38–41, 2013.

[13] Z. Kassas, J. Khalife, K. Shamaei, and J. Morales, "I hear, therefore I know where I am: Compensating for GNSS limitations with cellular signals," *IEEE Signal Processing Magazine*, pp. 111–124, September 2017.

[14] C. Yang, T. Nguyen, and E. Blasch, "Mobile positioning via fusion of mixed signals of opportunity," *IEEE Aerospace and Electronic Systems Magazine*, vol. 29, no. 4, pp. 34–46, April 2014.

[15] S. Fang, J. Chen, H. Huang, and T. Lin, "Is FM a RF-based positioning solution in a metropolitan-scale environment? A probabilistic approach with radio measurements analysis," *IEEE Transactions on Broadcasting*, vol. 55, no. 3, pp. 577–588, September 2009.

[16] Z. Kassas, J. Morales, and J. Khalife, "New-age satellitebased navigation – STAN: simultaneous tracking and navigation with LEO satellite signals," *Inside GNSS Magazine*, vol. 14, no. 4, pp. 56–65, 2019.

[17] J. Morales, P. Roysdon, and Z. Kassas, "Signals of opportunity aided inertial navigation," in *Proceedings of ION GNSS Conference*, September 2016, pp. 1492–1501.

[18] Z. Kassas, J. Morales, K. Shamaei, and J. Khalife, "LTE steers UAV," *GPS World Magazine*, vol. 28, no. 4, pp. 18–25, April 2017.

[19] M. Maaref, J. Khalife, and Z. Kassas, "Lane-level localization and mapping in GNSS-challenged environments by fusing lidar data and cellular pseudoranges," *IEEE Transactions on Intelligent Vehicles*, vol. 4, no. 1, pp. 73–89, March 2019.

[20] J. Morales, J. Khalife, and Z. Kassas, "GNSS vertical dilution of precision reduction using terrestrial signals of opportunity," in *Proceedings of ION International Technical Meeting Conference*, January 2016, pp. 664–669.

[21] J. Morales, J. Khalife, and Z. Kassas, "Opportunity for accuracy," *GPS World Magazine*, vol. 27, no. 3, pp. 22–29, March 2016.

[22] D. Salos, A. Martineau, C. Macabiau, B. Bonhoure, and D. Kubrak, "Receiver autonomous integrity monitoring of GNSS signals for electronic toll collection," *IEEE Transactions on Intelligent Transportation Systems*, vol. 15, no. 1, pp. 94–103, February 2014.

[23] Z. Kassas, V. Ghadiok, and T. Humphreys, "Adaptive estimation of signals of opportunity," in *Proceedings of ION GNSS Conference*, September 2014, pp. 1679–1689.

[24] J. Morales and Z. Kassas, "Optimal collaborative mapping of terrestrial transmitters: receiver placement and performance characterization," *IEEE Transactions on Aerospace and Electronic Systems*, vol. 54, no. 2, pp. 992–1007, April 2018.

[25] Z. Kassas and T. Humphreys, "Observability analysis of collaborative opportunistic navigation with pseudorange measurements," *IEEE Transactions on Intelligent Transportation Systems*, vol. 15, no. 1, pp. 260–273, February 2014.

[26] F. Knutti, M. Sabathy, M. Driusso, H. Mathis, and C. Marshall, "Positioning using LTE signals," in *Proceedings of Navigation Conference in Europe*, April 2015, pp. 1–8.

[27] K. Shamaei, J. Khalife, and Z. Kassas, "Performance characterization of positioning in LTE systems," in *Proceedings of ION GNSS Conference*, September 2016, pp. 2262–2270.

[28] M. Maaref and Z. Kassas, "Autonomous measurement outlier detection and exclusion for ground vehicle navigation with cellular signals and an IMU," *IEEE Transactions on Intelligent Vehicles*, 2019, submitted.

[29] J. Khalife, K. Shamaei, and Z. Kassas, "Navigation with cellular CDMA signals – part I: Signal modeling and software-defined receiver design," *IEEE Transactions on Signal Processing*, vol. 66, no. 8, pp. 2191–2203, April 2018.

[30] K. Shamaei, J. Khalife, and Z. Kassas, "Exploiting LTE signals for navigation: Theory to implementation," *IEEE Transactions on Wireless Communications*, vol. 17, no. 4, pp. 2173–2189, April 2018.

[31] K. Shamaei and Z. Kassas, "LTE receiver design and multipath analysis for navigation in urban environments," *NAVIGATION, Journal of the Institute of Navigation*, vol. 65, no. 4, pp. 655–675, December 2018.

[32] GPS Directorate, "Global positioning system standard positioning service performance standard (GPS SPS PS)," http://www.gps.gov/technical/ps/, September 2008.

[33] L. Heng, "Safe satellite navigation with multiple constellations: Global monitoring of GPS and GLONASS signal-in-space anomalies," Ph.D. dissertation, Stanford University, USA, 2012.

[34] H. Tong, G. Zhang, and G. Ou, "GNSS RAIM availability assessment for worldwide precision approaches," in *Proceedings of International Workshop on Multi-Platform/Multi-Sensor Remote Sensing and Mapping*, January 2011, pp. 1–4.

[35] A. Grosch, O. Crespillo, I. Martini, and C. Gunther, "Snapshot residual and Kalman filter based fault detection and exclusion schemes for robust railway navigation," in *Proceedings of European Navigation Conference*, May 2017, pp. 36–47.

[36] National instrument universal software radio peripheral-2954r. [Online]. Available: http://www.ni.com/en-us/support/model.usrp-2954.html

[37] (2018) Septentrio AsteRx-i V. [Online]. Available: https://www.septentrio.com/products